Chinese Chemical Letters 33 (2022) 3951–3954

Contents lists available at ScienceDirect

Chinese Chemical Letters

journal homepage: www.elsevier.com/locate/cclet

Inhibition of lithium dendrites and dead lithium by an ionic liquid additive toward safe and stable lithium metal anodes

Shengjie Zhang[a,1], Bin Cheng[a,1], Yanxiong Fang[a], Dai Dang[a], Xin Shen[b], Zhiqiang Li[a], Ming Wu[a], Yun Hong[a], Quanbing Liu[a,*]

[a] Guangzhou Key Laboratory of Clean Transportation Energy Chemistry, Guangdong Provincial Key Laboratory of Plant Resources Biorefinery, School of Chemical Engineering and Light Industry, Guangdong University of Technology, Guangzhou 510006, China
[b] Department of Chemical Engineering, Beijing Key Laboratory of Green Chemical Reaction Engineering and Technology, Tsinghua University, Beijing 100084, China

ARTICLE INFO

Article history:
Received 2 October 2021
Revised 1 November 2021
Accepted 5 November 2021
Available online 11 November 2021

Keywords:
Ionic liquid
Piperidinium
Lithium metal anode
Solid electrolyte interface
Lithium dendrites
Dead lithium

ABSTRACT

The uncontrolled growth of lithium dendrites and accumulation of "dead lithium" upon cycling are among the main obstacles that hinder the widespread application of lithium metal anodes. Herein, an ionic liquid (IL) consisting of 1-methyl-1-propylpiperidinium cation (Pp_{13}^+) and bis(fluorosulfonyl)imide anion (FSI^-), was chosen as the additive in propylene carbonate (PC)-based liquid electrolytes to circumvent the shortcoming of lithium metal anodes. The optimal 1% $Pp_{13}FSI$ acts as the role of electrostatic shielding, lithiophobic effect and participating in the formation of solid electrolyte interface (SEI) layer with enhanced properties. The *in-situ* optical microscopy records that the addition of IL can effectively inhibit the growth of lithium dendrites and the corrosion of lithium anode. This study delivers an effective modification to optimize electrolytes for stable lithium metal batteries.

In pursuit of reliable high-energy-density battery technologies beyond lithium-ion batteries (LIBs), safe and stable lithium metal anodes are the key components to pair with emerging cathode materials based on elemental sulfur and air [1–7]. The lithium metal anode presents an overwhelming advantage in energy density owing to its extremely high specific capacity (3860 mAh/g) and ultralow redox potential (−3.04 V) [8–11]. However, the widespread application of lithium metal anodes is hindered by the formation and accumulation of "dead lithium" upon battery cycling and unavoidable growth of lithium dendrites. These two major obstacles render lithium-metal-based batteries with rapid capacity decay, early cell failure, and internal short circuit [12–14]. All these phenomena threaten the battery safety and lower the system stability.

Recent advance in understanding the lithium-metal-based battery chemistries has revealed that the above issues of lithium metal anodes are directly related to the failure of solid electrolyte interphase (SEI). SEI is an electrically insulating and ionically conductive interface naturally formed in between the lithium metal and the electrolyte. Thus, electrolyte engineering through electrolyte additives [15–18] and new solvents/salts [19–21] has been regarded as an effective strategy to modulate the structure and properties of SEI. Among various electrolyte additives/solvents, ionic liquids (ILs) with multiple promising properties, such as great thermal, chemical, and electrochemical stabilities, low vapor pressure, non-flammability, and high ionic conductivity [22–24], have been proved to stabilize SEI and render the batteries with high coulombic efficiency and excellent cycling stability [20]. Particularly, the structural diversity and tunability of ILs allow delicate molecular design and further modulation of SEI structures and properties, which could then demonstrate a way to conquer the inherent challenges associated with lithium metal anodes.

Piperidine-based ILs have previously shown wide electrochemical potential windows and excellent adaptabilities to a large number of cathode materials such as olive-type lithium iron phosphates and layered lithium nickel/cobalt/manganese oxides [25–29], and therefore are promising candidates for electrolyte engineering and SEI reinforcement [30,31]. Therefore, 1-methyl-1-propylpiperidinium bis(fluorosulfonyl)imide ($Pp_{13}FSI$) was selected as an IL additive to reinforce the SEI and stabilize the lithium metal anode in a propylene carbonate (PC)-based liquid electrolyte. Different concentrations of $Pp_{13}FSI$ in LiFSI/PC electrolyte were prepared for evaluation with mass fractions of 0, 0.2%, 0.5%, 1%, 2% and 5%, which were denoted by PP0, PP0.2, PP0.5, PP1, PP2 and

* Corresponding author.
E-mail address: Liuqb@gdut.edu.cn (Q. Liu).
[1] These authors contributed equally to this work.

https://doi.org/10.1016/j.cclet.2021.11.024
1001-8417/

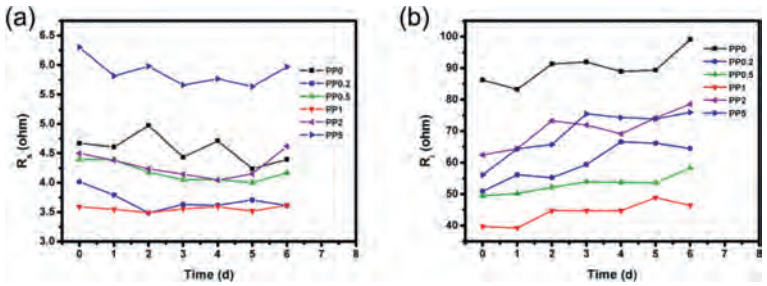

Fig. 1. The R_s and R_i values of EIS measurements of Li/Li cells with different LiFSI-PC/Pp_{13}FSI electrolytes.

PP5, respectively. The details of preparation are shown in experimental in the supplementary material.

Wettability, an essential property of electrolyte, can be evaluated by contact angle measurement of different electrolytes and polypropylene separators, as shown in Fig. S1 (Supporting information). The contact angles of different electrolytes are 70.3° for PP0.2, 65.4° for PP0.5, 68.5° for PP1, 69.7° for PP2, 75.9° for PP5, respectively. These values are similar to that of electrolyte without Pp_{13}FSI additive (69° for PP0), indicating that the addition of Pp_{13}FSI IL has no adverse effect on the wettability of electrolyte and separator.

To explore the contact behavior of Pp_{13}FSI addictive on the surface of lithium metal, Li|Li symmetrical batteries with the above electrolytes were assembled, kept for several days and conducted on the EIS measurements. The Nyquist plots of first six days' shelving are listed in Fig. S2 (Supporting information). The intercept at the Z' real axis in high frequency region corresponds to ohmic resistance of electrolyte solution (R_s). The suppressed semicircle in the low frequency region is related to the total interfacial resistance of two lithium electrodes (R_i). As shown in Fig. 1a, the solution resistances (R_s) of the symmetrical batteries maintain at low level. It should be noted that the addition of ionic liquid can slightly reduce the solution resistances of electrolytes till the concentration increases to 2 wt%. When the concentration reaches to 5 wt%, the solution resistance increases significantly because of the influence of a large amount of ionic liquid on the viscosity of electrolyte. The more beneficial effect of IL is reflected in the R_i values shown in Fig. 1b. The interfacial resistance of fresh battery decreases when IL is added with an optimized concentration about 1 wt%. During several days' shelving, the R_i values increases obviously. With the increase of IL proportion in electrolyte, the amplification of R_i decreases gradually, indicating that Pp_{13}FSI ionic liquid can slow down the side reaction between electrolyte and lithium metal.

To investigate the effects of IL additive, asymmetric batteries consisting of Li foil and Cu foil as electrodes were fabricated with the obtained electrolytes. The discharge conditions were set to 1 mAh/cm^2 with current density of 0.2 mA/cm^2, whereas the charge profiles ended when the potential reached 1 V *versus* Li/Li$^+$. The discharge process corresponds to Li deposition onto Cu foil, and the charge process is related to Li dissolution from Cu foil and deposition onto Li foil. The coulombic efficiency (CE) was defined as charge capacity divided by discharge capacity. The CEs of Li/Cu cells with different electrolytes are shown in Fig. 2. The initial CEs of the cells are 79% for PP0, 92% for PP0.2, 85% for PP0.5, 86% for PP1, 82% for PP2, and 78% for PP5, respectively. After 100 cycles, the CE of PP0 decreases to 47%, revealing a poor electrochemical stability. With addition of Pp_{13}FSI IL, the CEs are effectively improved. Especially for PP1, the CE maintains at 90% without any fluctuation during 100 cycles, confirming the importance of IL and its content.

Meanwhile, the voltage profiles of the above cells at 1st and 25th cycle (Fig. 3) reflect consistent conclusion in another way that

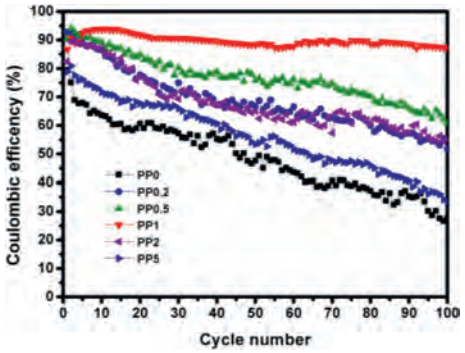

Fig. 2. The CEs of Li/Cu cells with different electrolytes.

PP1 cell exhibits the highest charge capacity at the given discharge capacity after 25 cycles. In the charge processes, the PP0 cell shows one more platform compared with the other cells with Pp_{13}FSI in the electrolytes, indicating that Pp_{13}FSI can effectively restrain the side reactions in the battery system. It has been clarified in the literature that the cation with nonpolar aliphatic chain engages electrostatic shielding effect and lithiophobic effect and the FSI$^-$ anion induces the formation of rigid SEI film. The overpotentials (voltage difference between charge and discharge platforms) of different cells at 1st and 25th cycles are shown in Figs. 3c and d. The overpotentials are 128 mV for PP0, 46 mV for PP0.2, 65 mV for PP0.5, 60 mV for PP1, 61 mV for PP2 and 95 mV for PP5, respectively. The lower overpotentials with Pp_{13}FSI cells reveal that the enhanced interfacial construction with the synergistic effect of the cation and anion of Pp_{13}FSI. After 25 cycles, these values change to 144, 68, 63, 42, 56 and 68 mV, respectively. PP1 cell exhibits the lowest overpotential, supporting an optimal amount of IL, which affected by the advantages and disadvantages of ILs comprehensively. This regularity is consistent with the previous EIS results.

The surface reaction can be directly observed by the surface and cross-sectional SEM images of the Li anodes after 50 cycles at 0.2 mA/cm^2 in PP0 and PP1 electrolytes, as shown in Fig. 4. The Li anode of PP0 cell in Figs. 4a and b displays that rod-like Li grow on the whole surface of the electrode, forming a rough surface. The cross-sectional image in Fig. 4c shows a thick "dead Li" layer with a distinct boundary with bulk lithium foil and Li dendrites grew on the surface of "dead Li" layer (circled in red). In contrast, a smooth surface can be observed in the anode of PP1 cell shown in Figs. 4d–f. Moreover, there seems to be no obvious stratification on the surface of the cross-sectional image in Fig. 4f, indicating that no obvious "dead Li" layer is formed. These morphological differences are the results of synergistic effect of IL, which makes lithium uniformly deposit on the lithium anode and effectively avoids lithium dendrites grew by local deposition.

The effects of ionic liquid on the surface improvement of lithium anode can be directly observed by *in-situ* optical microscopy recorded in Figs. S3–S5 and movies S1 (PP0) and S2 (PP1)

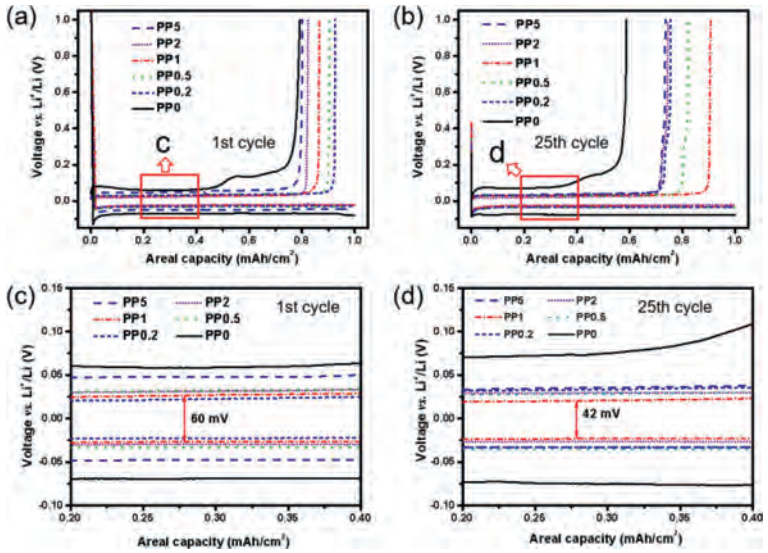

Fig. 3. (a, b) The charge-discharge profiles and (c, d) over potential of Li/Cu cells with different electrolytes.

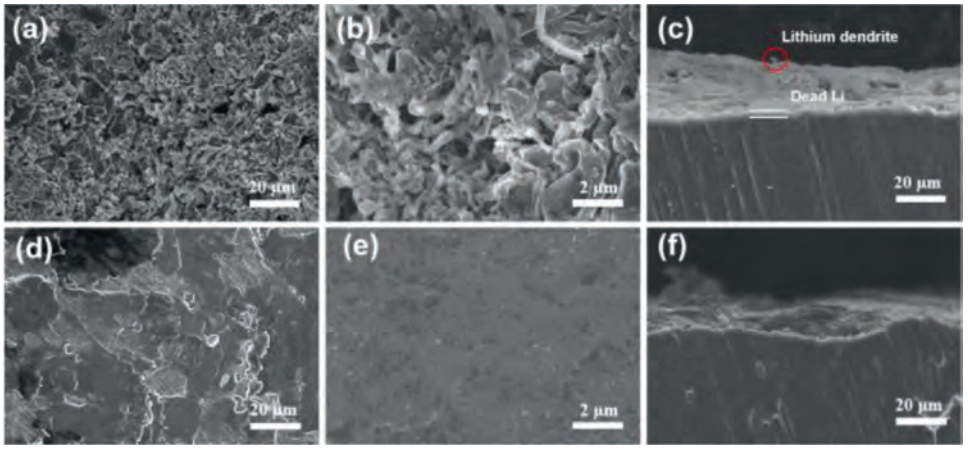

Fig. 4. The surface and cross-sectional SEM images of the Li metal electrodes that underwent 50 cycles at 0.2 mA/cm^2 in (a–c) PP0 and (d–f) PP1 electrolytes.

(Supporting information). At beginning, the surface of lithium electrode is smooth without any protuberance in LiFSI-PC or LiFSI-1%Pp_{13}FSI/PC electrolyte. Plating 30 min with current density of 2.0 mA/cm^2, the two systems exhibit similar phenomena that mosslike lithium deposits on the surface. After stripping 30 min, most of the mosslike lithium disappears in the LiFSI-1%Pp_{13}FSI/PC electrolyte test cell. In contract, the LiFSI-PC system leaves more lithium behind. This difference is consistent with the result of coulomb efficiency. With the formation of SEI on the surface of lithium in the first cycle, lithium deposition and dissolution gradually decrease during the second and third cycle for LiFSI-1%Pp_{13}FSI/PC system. But for the LiFSI-PC system, lithium deposition does not happen on the top, but on the bottom of the lithium left in the first cycle, resulting in jacking up the previous lithium to form a "dead Li" layer, which decomposes and suspends in electrolyte in subsequent cycles, without any capacity contribution. Last but not least, the surface morphology of LiFSI-PC system keeps stable when the current density increases in second and third cycle, indicating the possibility of excellent rate performance. Comparing the two movies, we can conclude that the addition of 1% Pp_{13}FSI in electrolyte can induce the formation of a special SEI film, thereby effectively prevent the formation of "dead Li".

The chemical compositions of SEI layers of lithium anode in PP0 and PP1 systems after 50 cycles are analyzed by X-ray photoelectron spectroscopy (XPS), as shown in Fig. S6 (Supporting information). In C 1s spectra (Figs. S6a and d), the peaks located at 288.8, 286.5 and 284.8 eV are related to CO_3^{2-}, COR and C–C bonds, respectively, which can be attributed to the decomposition of PC solvent. The N 1s spectrum of PP0 (Fig. S6b) maintains a peak related to FSI^- anions with slight increase in intensity during 50 cycles. Compared to PP0, two extra peaks appear at 397.8 and 398.0 eV in the N 1s spectrum of PP1, corresponding to the Pp_{13}^+ and Li_3N. After 50 cycles, the intensities of Pp_{13}^+, FSI^- and Li_3N peaks increase obviously, indicating that Pp_{13}FSI is involved in the formation of SEI film. The same phenomenon occurs in the F 1s spectrum (Figs. S6c and f). A new peak at 688.4 eV corresponding to CF_3 group emerges and increases during 50 cycles.

We proposed a promising method to solve the issue of Li metal electrode *via* introducing Pp_{13}FSI as an electrolyte additive to improve the stability of interface between electrolyte and lithium anode, result in effectively inhibiting the growth of lithium dendrites and "dead Li" layer. The optimal 1 wt% Pp_{13}FSI IL acts as the role in balancing electrostatic shielding, lithiophobic effect and participating in the formation of SEI layer that can enhance the performance of electrode. Furthermore, the Pp_{13}FSI can avoid the inherent shortcomings, such as high viscosity and poor wettability. we firmly believe that these findings would be a great beneficial for

the different electrochemical systems such as Li-S batteries and Li-air batteries.

Declaration of competing interest

The authors declare that they have no known competing financial interests or personal relationships that could have appeared to influence the work reported in this paper.

Acknowledgments

This work was supported by the Key Research and Development Program of Guangdong Province (No. 2020B090919005), the National Natural Science Foundation of China (Nos. 21975056, 52002079 and U1801257), Pearl River Science and Technology New Star Project (No. 201806010039).

Supplementary materials

Supplementary material associated with this article can be found, in the online version, at doi:10.1016/j.cclet.2021.11.024.

References

[1] M. Gao, H. Li, L. Xu, et al., J. Energy Chem. 59 (2021) 666–687.
[2] C. Wu, J. Lou, J. Zhang, et al., Nano Energy 87 (2021) 106081.
[3] L. Ma, J. Cui, S. Yao, et al., Energy Storage Mater. 27 (2020) 522–554.
[4] X. Shen, Y. Li, T. Qian, et al., Nat. Commun. 10 (2019) 900.
[5] R. Xu, X. Shen, X.X. Ma, et al., Angew. Chem. Int. Ed. 60 (2021) 4215.
[6] X. Shen, X.Q. Zhang, F. Ding, et al., Energy Mater. Adv. (2021) 1205324.
[7] Q.K. Zhang, X.Q. Zhang, H. Yuan, J.Q. Huang, Small Sci. 1 (2021) 2100058.
[8] J. Wang, B. Ge, H. Li, et al., Chem. Eng. J. 420 (2021) 129739.
[9] F. Wu, Y. Yu, Joule 2 (2018) 815–817.
[10] X. Yan, H. Zhang, M. Huang, M. Qu, Z. Wei, ChemSusChem 12 (2019) 2263–2270.
[11] T. Liu, X.L. Feng, X. Jin, et al., Angew. Chem. Int. Ed. 58 (2019) 18240.
[12] K.D. Victoria, B. Christopher, K. Omichi, et al., Science 362362 (2018) 1144–1148.
[13] N. Chen, Y. Dai, Y. Xing, et al., Energy Environ. Sci. 10 (2017) 1660–1667.
[14] H.D. Nguyen, G.T. Kim, J. Shi, et al., Energy Environ. Sci. 11 (2018) 3298–3309.
[15] N.A. Sahalie, A.A. Assegie, W.N. Su, et al., J. Power Sources 437 (2019) 226912.
[16] X.Q. Zhang, X.B. Cheng, X. Chen, C. Yan, Q. Zhang, Adv. Funct. Mater. 27 (2017) 1605989.
[17] Y. Wang, Z.J. Wang, L. Zhao, et al., Adv. Mater. 33 (2021) 2008133.
[18] B. Yun, Y.B. He, W. Lv, et al., Adv. Mater. 28 (2016) 6932–6939.
[19] J. Zhao, L. Liao, F. Shi, et al., J. Am. Chem. Soc. 139 (2017) 11550–11558.
[20] A. Basile, A.I. Bhatt, A.P. O'Mullane, Nat. Commun. 7 (2016) 11794.
[21] N.W. Li, Y.X. Yin, J.Y. Li, C.H. Zhang, Y.G. Guo, Adv. Sci. 4 (2017) 1600400.
[22] K. Yamaguchi, Y. Domi, H. Usui, M. Shimizu, H. Sakaguchi, J. Electrochem. Soc. 166 (2019) A268–A276.
[23] A. Tsurumaki, H. Ohno, S. Panero, M. Navarra, Electrochim. Acta 293 (2019) 160–165.
[24] Q. Yang, Z. Zhang, X. Sun, et al., Chem. Soc. Rev. 47 (2018) 2020–2064.
[25] D. Yoo, K.J. Kim, J.W. Choi, Adv. Energy Mater. 8 (2018) 1702744.
[26] K. Kim, Y.H. Cho, H.C. Shin, J. Power Sources 225 (2013) 113–118.
[27] J. Reiter, M. Nadherna, R. Dominko, J. Power Sources 205 (2012) 402–407.
[28] X.N. Pan, J. Hou, L. Liu, et al., Ionics 23 (2017) 3151–3161 (Kiel).
[29] K.S. Korf, Y. Lu, Y. Kambe, L.A. Arche, J. Mater. Chem. A 2 (2014) 11866–11873.
[30] S.J. Zhang, J.H. Li, N.Y. Jiang, et al., Chem. Asian J. 14 (2019) 1–6.
[31] J.F. Ding, R. Xu, C. Yan, et al., J. Energy Chem. 59 (2021) 306–319.